Research Article

Lei Yang* and Yi-Zhu He

Modeling and simulation of dynamic recrystallization behavior for Q890 steel plate based on plane strain compression tests

https://doi.org/10.1515/phys-2020-0166
received November 28, 2019; accepted June 7, 2020

Abstract: In view that the traditional dynamic recrystallization (DRX) model cannot effectively predict the DRX process in the hot deformation process of sheet metal, DRX behavior modeling and simulation of q890 steel plate based on the plane strain compression test are designed. The plane strain thermal simulation tests were performed at 1,223–1,373 K and the strain rates of $1–50^{-1}$ on Gleeble-3500 thermal–mechanical simulator. The flow stress curves were well smoothed. The stress–strain data were investigated for the analysis of the dynamic recrystallization in the process of thermal deformation. The activation energy of DRX was calculated as $Q = 394.53$ kJ/mol by the simulation data. The equation of peak strain was developed with the flow stress data by the Zener–Hollomon parameter. The DRX transformation fraction of Q890 steel was studied, and the DRX kinetics equation was developed by the Avrami equation. The experimental data are in good agreement with the calculated values, which proves the reliability of the DRX model and can be widely used in real life.

Keywords: plane strain, flow stress, thermal deformation, dynamic recrystallization

1 Introduction

Continuous heat processing of metallic materials requires the evaluation of product quality with a given technology. Therefore, the predictions of the heat processing results are important for online process or off-line process. During hot deformation, dynamic recovery (DRV) and dynamic recrystallization (DRX) are the main mechanism to balance the work hardening. The model of the thermomechanical processing of steels is established by the thermomechanical parameters such as temperatures and strains. The major influence on microstructure evolution is the dynamic recrystallization that occurred under given conditions. Some methods for modeling the progress of dynamic recrystallization were introduced to describe the softening. The procedure was established through the analysis of stress–strain curves. McQueen and Ryan [1] discussed the dynamic recrystallizaion of different metallic materials including micro-alloyed steels and stainless steels. Based on the research of the critical strain, the initiation of dynamic recrystallization is to be determined. Many authors also made contribution for the development of models, such as Jonas et al. [2], Rossi and Sellars [3], and Khoddam and Hodgson [4]. Most of the models are established by torsion tests or cylinder specimen compression tests [5–7]. Compared with the cylindrical compression test, there is no bulging phenomenon in the process of plane strain compression, and the frictional force of plane strain compression contact surface is smaller. In addition, the stress state of the plane strain experiment is closer to that of the hot rolling plate process. The DRX is a complex thermomechanical process, and the aim to this study is to determine the critical strain and the critical stress in the DRX, which can be disposed in many ways [8–10]. The hardening and recrystallization behaviors vary for different materials [11,12]. Therefore, it is necessary to study the parameters of DRX for specific materials.

The main aim of this study is to analyze the hot deformation behavior of Q890 micro-alloyed steels, which can be used for die materials. Based on the plane strain compression tests, the effects of the critical strain, deformation temperature, and strain rate were investigated, which are used for developing the kinetics model

* **Corresponding author: Lei Yang,** School of Materials Science and Engineering, Anhui University of Technology, Ma'anshan 243002, China, e-mail: yangleitown@163.com
Yi-Zhu He: School of Materials Science and Engineering, Anhui University of Technology, Ma'anshan 243002, China

of dynamic recrystallization for Q890 micro-alloyed steels. The integrated equations are proposed to predict the softening behaviors induced by dynamic recrystallization in the studied material.

2 Experiments

The chemical compositions of Q890 steel are as follows (wt%): C, 0.16; Si, 0.29; Mn, 1.27; Cr, 0.35; Mo, 0.51; Ni, 0.38; Fe, balance. The simulated sample with the length of 20 mm, the width of 15 mm, and the height of 10 mm was machined from the hot rolling plate. To reduce friction and to guarantee the parallel degree, which could produce an effect on experiment precision of stress–strain curves, the sample was carefully polished. The plane strain compression tests, which are used to simulate flat rolling as shown in Figure 1, were conducted on Gleeble 3500 testing machine. The deformation forces, stain, and the metal flow direction of the plane strain simulation are all in the same direction as those found in the flat rolling. In the process of plane strain experimental, the conditions of stress–strain state are closer to flat rolling than that of the cylindrical compression test. Compared with the cylindrical compression test, the bulging and the high friction can be minimized in the plane strain compression test. By using high resistance anvils, less than 1% thermal gradient from anvil to anvil can be obtained with the sample size used in this experiment. Test process diagram is shown in Figure 2. The specimens were first heated at a heating rate of 5 K/s to a soaking temperature of 1,473 K and held for 5 min, thus making the austenitic microstructure homogenizing treated. Then, the temperature of sample was decreased to a certain temperature at a rate of 5 K/s, holding 30 s at uniform temperature before deformation.

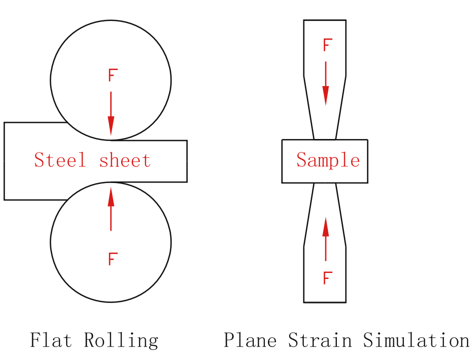

Figure 1: Schematic diagram of plane strain simulation.

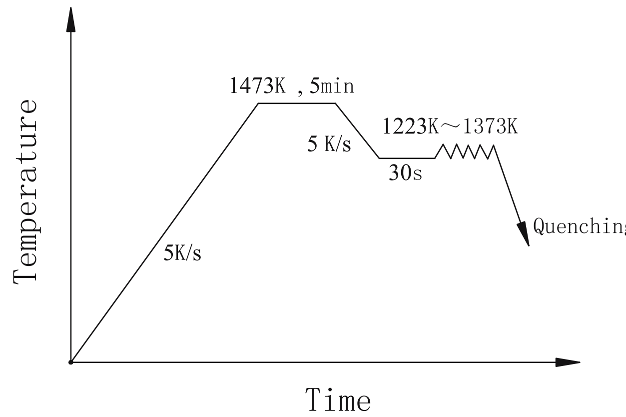

Figure 2: Experimental process of plane strain simulation.

The compression tests carried out at a height reduction of 60%. The simulation temperatures were 1,223, 1,273, 1,332, and 1,373 K. The test parameters of strain rates were $1\,s^{-1}$, $5\,s^{-1}$, 10^{-1}, and 50^{-1}. GLEEBLE-3500 automatically collects the real stress, true strain, pressure, temperature, displacement, time, and other experimental data and then draws the true stress–true strain curve by Origin software.

3 Results and discussion

3.1 Flow stress behavior strain and strain rate

The true stress–strain curves of Q890 steel under different deformation conditions are shown in Figure 3. According to the data of stress–strain curves, it is need to separate the part of DRV and DRX. It is also found that the flow stress decreases rapidly with the lower deformation temperature for a certain strain rate. In the process of DRV, it is an ascending trend that the stress increases with strain. However, while the DRX occurred in a certain compression test, the flow stress decreased in critical condition. From the curves show in Figure 3, it has three distinct stages obviously. In the first stage, the flow stress increases rapidly to a critical value because of work hardening behavior in the deformed steel. In the second stage, the dynamic recrystallizaion is initiated at a critical strain, which results in more softening to balance the work hardening. A maximum value of stress can be found in the stress–strain curves. In the third stage, in the continuing dynamic recrystallizaion, the curves have a steady state. The main factor is that the temperature and

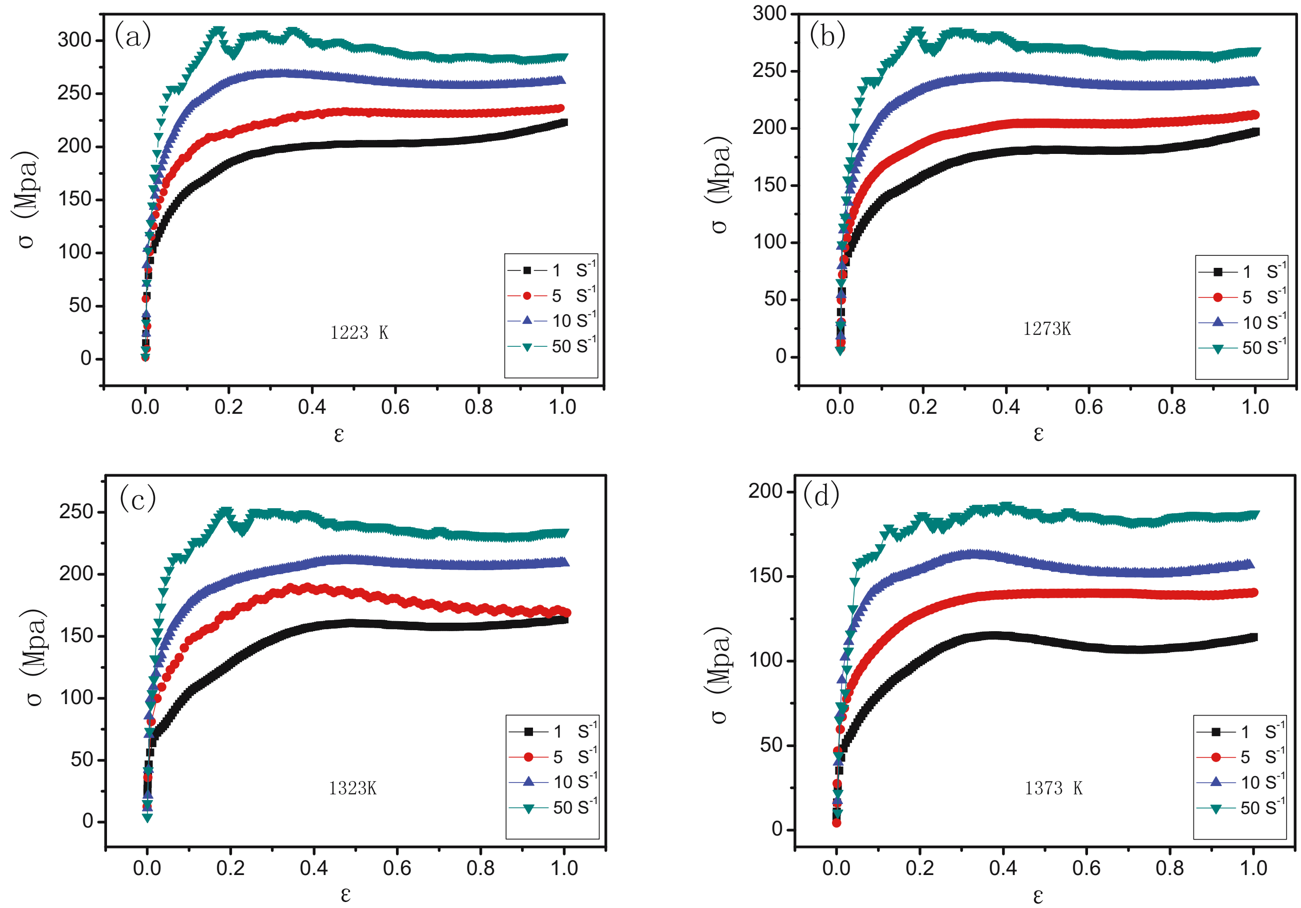

Figure 3: Flow stress curves of plane strain simulation under temperatures of (a) 1,223 K, (b) 1,273 K, (c) 1,323 K, and (d) 1,373 K.

strain rate affected the DRX. The DRX occurs more rapidly in a certain strain rate, while the deformation temperature increases. Therefore, a typical curve of the dynamic recrystallizaion softening includes a peak stress value and a steady-state process. At constant strain rate, the higher the temperature is, the more likely it is to induce grain boundary migration of DRX. In contrast, under the condition of the lower strain rate, the dynamic recrystallizaion would be more likely to happen [13–15].

During DRX, the main influencing factors are the temperature and strain rate, which are used in the hot deformation process of the plane strain experimental. When the parameter of the strain rate is constant, the higher the hot deformation temperature is, the faster the DRX occurs. Therefore, once DRX occurs, there must be a peak stress in the flow stress curve. The stress value tends to be stable. DRX usually occurs at the boundary of the original deformed particles. Normally, lower strain rate and higher deformation temperature are considered to contribute to the initiation of DRX in hot deformation.

3.2 The initiation of DRX

In the early stage of high temperature deformation, the specimen is in elastic deformation, which should be removed before processing the data. The starting point of fitting data was at the 2% of the total strain, which was considered that the stress value on sample was over the yield stress. As shown in Figure 4(a), an example of an experimental curve was given. The experimental parameters of compression were at 1,273 K and a strain rate of 10 s^{-1}. The ninth-order polynomial fitting curve starts from σ, which was decided by the yield principle mentioned earlier. The fitting curve was precise within about 1% as shown in Figure 4(b). The reasons of experimental errors were due to temperature fluctuations and load measurement, as well as nonlinear plastic deformation process.

In the DRX, the stress corresponding to the critical strain is the critical stress. To determine the values of the critical stress, the strain hardening rate ($\theta = d\sigma/d\varepsilon$) was calculated from the flow curves. This method was employed to define the critical stress as shown in

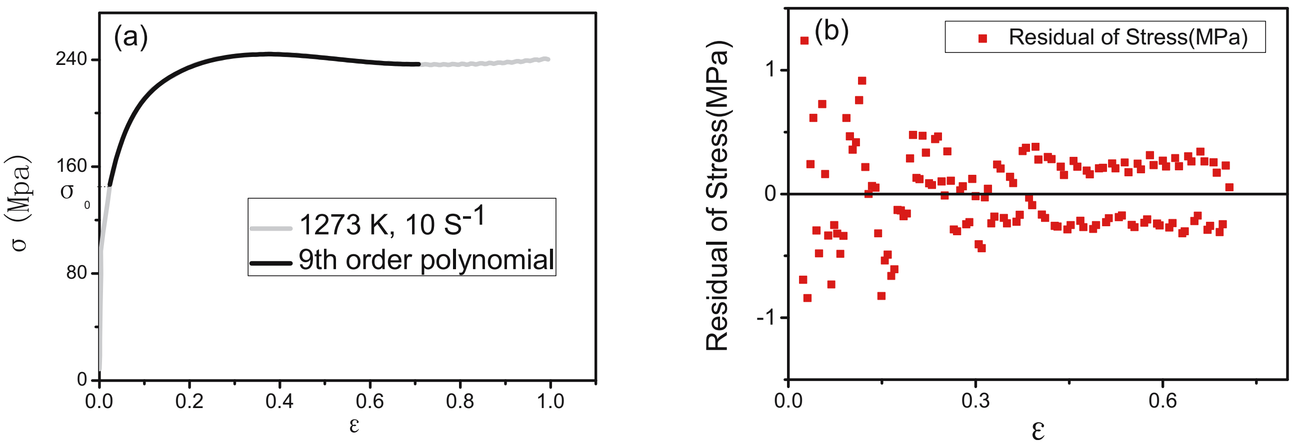

Figure 4: Fitting of the experimental flow stress curve at 1,273 K and a strain rate 10 S^{-1}. (a) The curve was fitted with a ninth-order polynomial. (b) The errors of the fitting values.

Figure 5. If DRX occurs, the rate of reduction of hardening rate will decrease. The critical value of the hardening curve is defined as the critical stress. When the value of $\partial^2\theta/\partial\sigma^2$ is zero, the critical stress σ_c could be found under the condition of $\theta = 0$. Once the strain on the specimen is over the critical strain ε_c corresponding to the critical stress, the DRX will be initiated, which causes more softening. The peak stress σ_p is the maximum stress in the experiment. The value of the peak stress can be defined by the hardening rate θ falling to zero. By using this method, 16 flow curves were analyzed to identify the initiation of the critical stress. According to the critical stress, the corresponding critical strain could be obtained from the flow stress curves. The values of the critical stress and peak stress were presented in Table 1. The ratio between the critical stress and peak stress is linear, depending on the temperature and the strain rate. Therefore, the trends were determined as $\sigma_c = 0.94\sigma_p$ as shown in Figure 6. There is a linear relationship between the critical stress σ_c and the peak stress σ_p.

Figure 7a and b shows variation of the critical stress σ_c with $1/T$ for different strain rates and with $\dot{\varepsilon}$ at different T. This figure shows that the critical stress is dependent on both strain rate and temperature. The slope of each plot in Figure 7 shows that the critical stress is sensitive to reciprocal of temperature range of 7.28×10^{-4} to $8.18 \times 10^{-4}\,K^{-1}$ and strain rate range of $1–50\,s^{-1}$. At the same temperature, the critical stress growth decreases with the

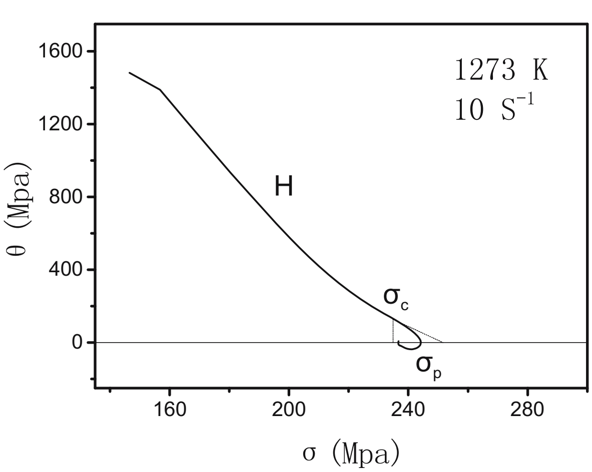

Figure 5: Hardening exponent θ versus flow stress.

Table 1: Values of ε_p, σ_p, ε_c, and σ_c under different plane strain experimental conditions

Strain rate (s^{-1})	Temperature (K)	ε_p	σ_p (Mpa)	ε_c	σ_c (Mpa)
1	1,373	0.375	115.16	0.270	109.76
	1,323	0.490	160.64	0.366	155.37
	1,273	0.522	181.28	0.401	179.28
	1,223	0.512	202.82	0.344	198.67
5	1,373	0.414	139.50	0.362	138.46
	1,323	0.354	187.76	0.273	180.48
	1,273	0.445	204.26	0.362	201.30
	1,223	0.476	233.31	0.384	229.62
10	1,373	0.327	162.68	0.221	156.30
	1,323	0.461	211.29	0.372	207.05
	1,273	0.355	244.24	0.245	239.30
	1,223	0.309	267.94	0.217	262.00
50	1,373	0.225	185.68	0.151	177.31
	1,323	0.253	247.89	0.180	238.59
	1,273	0.218	282.23	0.157	268.12
	1,223	0.213	312.69	0.178	290.62

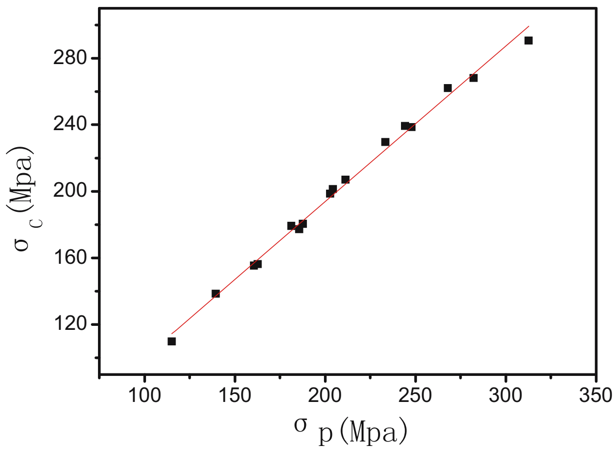

Figure 6: The critical stress versus the peak stress.

increase of the strain rate as shown in Figure 7b, which also shows that the increase of internal distortion energy caused by the acceleration of deformation rate promotes the start-up of DRX. Under the condition of high strain rate, the nucleation mode of recrystallization is different from that of the low strain rate.

3.3 Arrhenius equation for flow behavior with DRX

In the hot working process of steel plate, the occurrence of DRX is due to the accumulation of distortion energy in metal caused by work hardening during thermal deformation. While the accumulated energy exceeds the critical value required for DRX, DRX occurs in the deformed grain boundary. The activation energy of DRX, which is the important parameter for the initiation of DRX, could be calculated from the stress–strain curves. The Arrhenius equation is mostly used to study the thermal deformation behavior and deformation activation energy in thermal simulation process [16,17]. In this study, the method is also used to discuss the thermal simulation of plane strain and to establish the DRX constitutive equation of Q890 hot rolled plate during hot deformation. To construct DRX equation, the most important Zener–Hollomon (Z) parameter is introduced, which is expressed in equation (1). The Z parameter is considered as the function of temperature and strain rate on DRX during hot deformation [18]. With the increase of Z parameter, the grain size after DRX decreased, but when the strain rate exceeded the critical value, the grain size increased [19]. The DRX behavior in the process of high temperature deformation can be studied by Z-parameters in both compression and tension states [20]. The Arrhenius equation shown in equation (2) is used to calculate the activation energy of DRX. The gas constant R is 8.31 J/mol K, and the stress factor is 0.012 MPa^{-1}.

$$Z = \dot{\varepsilon}\exp\left(\frac{Q}{RT}\right) \tag{1}$$

$$\dot{\varepsilon} = A_1\{\sinh(\alpha\sigma)\}^n \exp(-Q/RT) \tag{2}$$

When the strain rate is constant and $1/T$ is a variable, the derivation of the equation (2) is obtained to construct the DRX activation energy equation expressed as $Q = Rn\left[\frac{\partial[\ln\sinh(\alpha\sigma_p)]}{\partial(1/T)}\right]\Big|_{\dot{\varepsilon}} = RnG$. When the temperature is constant and $\ln\sinh(\alpha\sigma_p)$ is a variable, the result of derivation of equation (2) is expressed as $n = \frac{\partial\ln\dot{\varepsilon}}{\partial[\ln\sinh(\alpha\sigma_p)]}\Big|_T$. Since the activation energy Q and

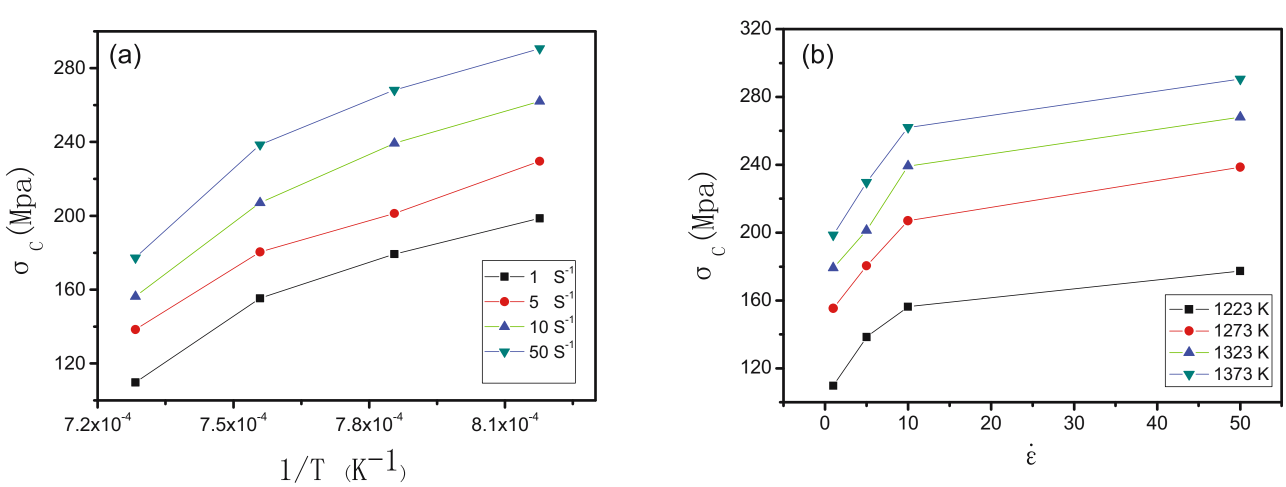

Figure 7: Variation of (a) the critical stress σ_c with $1/T$ for different strain rates and (b) with $\dot{\varepsilon}$ at different T values.

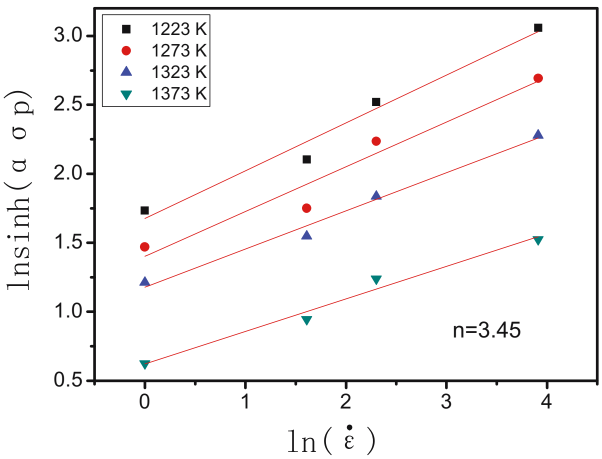

Figure 8: The relationship between $\ln \sinh(\alpha\sigma_p)$ and $\ln \dot{\varepsilon}$.

the stress exponent n are material constants, $\ln \sinh(\alpha\sigma_p)$ was used to plot with $\ln \dot{\varepsilon}$ and $1/T$, respectively. The results are shown in Figures 8 and 9. The average slope values are $n = 3.45$ and $G = 13{,}778$. The activation energy Q of DRX is 394.53 kJ/mol. The larger the deformation activation energy, the more difficult the DRX is. The activation energy of DRX is affected by the carbon content and alloy elements in steel.

The parameters Z and $\{\sinh(\alpha\sigma)\}^n$ were calculated by the data of 16 flow stress curves, combing equations (1) and (2). The result is shown in Figure 10, and thus, A_1 value is 9.75×10^{13}.

With the data of 16 flow stress curves, the process of DRX could be considered with the thermal parameter Z that is combined with the stress, the strain rate, and the temperature. When the strain rate and temperature are constant, the occurrence state of DRX can be judged under different strain conditions.

3.4 DRX kinetic model

When the strain rate is constant, the DRX fraction can be constructed by the Avrami equation, as shown in equation (3).

$$X_D = 1 - \exp\left[-0.693\left(\frac{\varepsilon - \varepsilon_c}{\varepsilon_p}\right)^m\right] \tag{3}$$

The value of the peak stress is mainly related to the strain rate and the temperature [21]. So the value of the peak stress can be expressed as $\varepsilon_p = a(Z/A_1)^b$. The linear relationships between $\ln(\varepsilon_p)$ and $\ln(Z/A_1)$ were fitted out as show in Figure 11. The function expression is $\varepsilon_p = 0.197(Z/A_1)^{0.106}$. According to the data of flow stress curves, the average value of $\varepsilon_c/\varepsilon_p$ is 0.6.

During hot deformation, when DRX occurs, the relationship between the DRX fraction and the stress can be expressed as $X_D = \frac{\sigma_p - \sigma^{dx}}{\sigma_p - \sigma_{ss}^{dx}}$ [22]. The parameter of σ^{dx} is the instantaneous stress value in the hot deformation process [23–25]. When work hardening and DRX softening reach dynamic equilibrium, the flow stress value tends to a steady-state stress value as σ_{ss}^{dx}. The linear relationships between $\ln\ln\left(\frac{1}{1 - X_D}\right)$ and $\ln\left(\frac{\varepsilon - \varepsilon_c}{\varepsilon_p}\right)$ were fitted out as shown in Figure 12. The average slope value is $m = 2.57$.

The DRX kinetics model can be obtained by the determined m value as shown in equation (4).

$$X_D = 1 - \exp\left[-0.693\left(\frac{\varepsilon - \varepsilon_c}{\varepsilon_p}\right)^{2.57}\right] \tag{4}$$

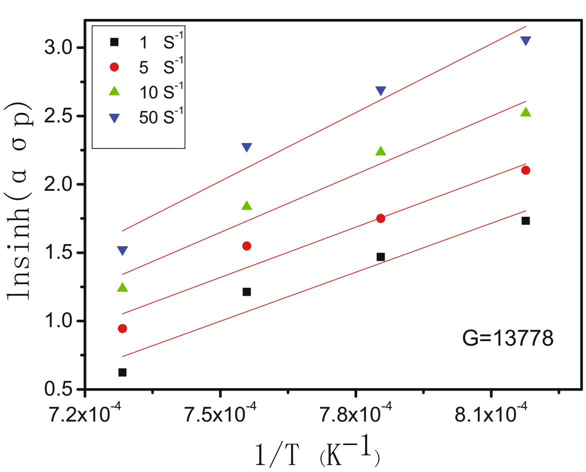

Figure 9: The relationships between lnsinh(ασp) parameter and $1/T$.

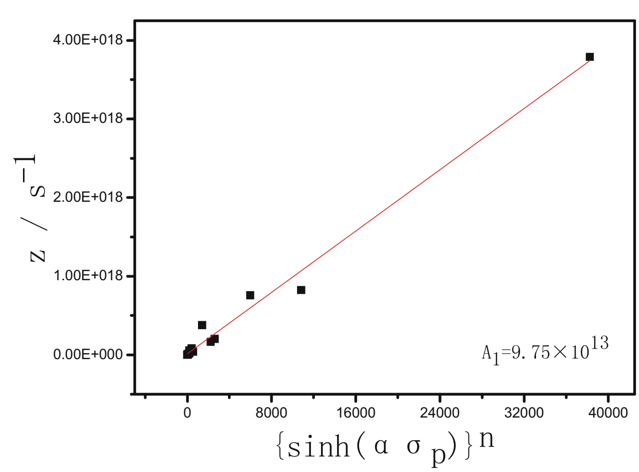

Figure 10: The relationship between Z parameter and $\{\sinh(\alpha\sigma)\}^n$.

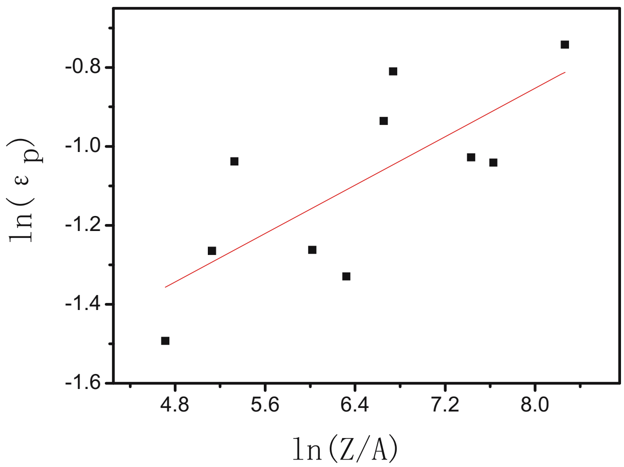

Figure 11: The relationship between $\ln(\varepsilon_p)$ and $\ln(Z/A_1)$.

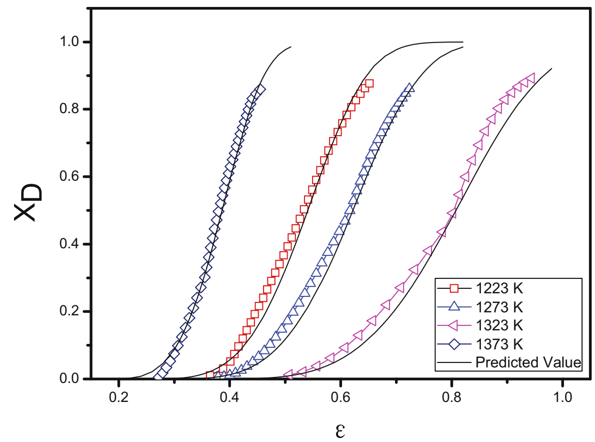

Figure 13: Comparison of calculated value with experimental ones ($\dot{\varepsilon}$ = 1s^{-1}).

To verify the accuracy of the model, the strain rate of 1 S^{-1} was compared with the simulated values shown in Figure 13. The computed results are in good agreement with the actual values, which shows that the DRX model constructed in this article can effectively predict the DRX evolution process of Q890 steel during the plate hot deformation [26,27].

The deformation process of plane strain experiments is closer to the deformation process of plate hot rolling when compared with the compression process of cylindrical specimen [28]. Therefore, the dynamic model constructed in this article is more suitable for predicting the DRX process of plate hot deformation. Through the GLEEBLE-3500 testing machine, the true stress–strain curves under different deformation conditions were obtained by isothermal compression of q890 steel plate. It was found that the alloy is prone to DRX under the

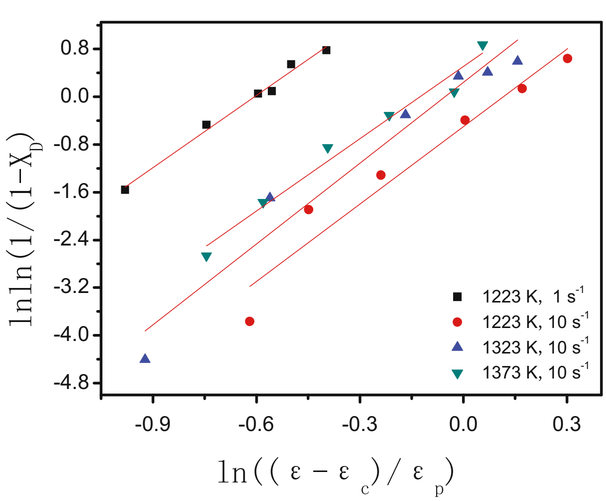

Figure 12: The relationship between $\ln\ln\left(\frac{1}{1-X_D}\right)$ and $\ln\left(\frac{\varepsilon-\varepsilon_c}{\varepsilon_p}\right)$.

condition of low strain rate, and the stress–strain curve is of DRX type. When the strain rate is high, the alloy is prone to DRV, and the stress–strain curve is of DRV type; the alloy has positive strain rate sensitivity.

4 Conclusions

In this article, DRX behavior modeling and simulation of q890 steel plate based on the plane strain compression test are proposed. Plane strain hot compression tests of Q890 hot rolled steel plate was carried out under different strain rates and deformation temperatures. In the process of the plane strain thermal simulation experiment, the main factors affecting DRX are strain rate and deformation temperature during hot deformation. Normally, the lower the strain rate and the higher the deformation temperature, the more likely it is to happen DRX. The trend chart between hardening exponent and stress was established by analyzing the data of the stress curves. Thus, the relationship between the critical stress and the peak stress is determined as $\sigma_c = 0.94\sigma_p$.

The DRX occurs when the accumulated energy of thermal deformation exceeds the activation energy of DRX. The effect of strain rate and temperature on DRX during hot deformation can be studied by the parameter Z. The activation energy of DRX of Q890 steel plate is Q = 394.53 kJ/mol. The DRX kinetics model of Q890 hot rolled steel plate during plane strain thermal simulation was established by using the Avrami equation. By comparing the simulated data with the actual data, the results are in good agreement. The model can effectively predict the DRX process in the hot deformation process of plate metal. Also, SEM and TEM can also be used to study the phase transformation and the second-phase particles in the process of thermal deformation and to further reveal the evolution rule of microstructure.

Acknowledgments: This work was supported by the Natural Science Foundation of Anhui Provincial Education Department (No. KJ2017A068).

References

[1] Mcqueen HJ, Ryan ND. Constitutive analysis in hot working. Mater Sci Eng A. 2002;322(1–2):43–63.
[2] Jonas JJ, Quelennec X, Jiang L, Martin É. The Avrami kinetics of dynamic recrystallization. Acta Mater. 2009;57(9):2748–56.
[3] Rossi PLO, Sellars CM. Quantitative metallography of recrystallization. Acta Mater. 1997;45(1):137–48.
[4] Khoddam S, Hodgson PD. The need to revise the current methods to measure and assess static recrystallization behavior. Mech Mater. 2015;89:85–97.
[5] Quan GZ, Li GS, Chen T, Wang YX, Zhang YW, Zhou J. Dynamic recrystallization kinetics of 42CrMo steel during compression atdifferent temperatures and strain rates. Mater Sci Eng A. 2011;528:4643–51.
[6] Xu Y, Tang D, Song Y, Pan X. Dynamic recrystallization kinetics model of X70 pipeline steel. Mater Des. 2012;39:168–74.
[7] Santosh K, Aashranth B, Dipti S, Davinci MA, Borah U, Bhaduri AK. Influence of nitrogen on kinetics of dynamic recrystallization in Fe–Cr–Ni–Mo steel. Vacuum. 2018;156:20–9.
[8] Soheil S. Determination of flow stress and the critical strain for the onset of dynamic recrystallization using a hyperbolic tangent function. Mater Des. 2014;54:390–3.
[9] Aranas C, Foul A, Guo B, Fall A, Jahazi M, Jonas J. Determination of the critical stress for the initiation of dynamic transformation in commercially pure titanium. Scr Mater. 2017;133:83–5.
[10] Wang J, Yang HT, Wang XG, Xiao H. A new mathematical model for predicting flow stress up to the critical strain during hot deformation. Mater Des. 2015;65:637–43.
[11] Zhang D, Liu YZ, Zhou LY, Han Q, Jiang B, Li ZZ. Dynamic recrystallization behavior of GCr15SiMn bearing steel during hot deformation. J Iron Steel Res Int. 2014;21:1042–8.
[12] Luo J, Wang LF, Liu SF, Li MQ. The correlation between the flow behavior and the microstructure evolution during hot working of TC18 alloy. Mater Sci Eng A. 2016;654:213–20.
[13] Chen MS, Yuan WQ, Li HB, Zou ZH. New insights on the relationship between flow stress softening and dynamic recrystallization behavior of magnesium alloy AZ31B. Mater Charact. 2019;147:173–83.
[14] Zhao B, Zhao T, Li G, Lu Q. The kinetics of dynamic recrystallization of a low carbon vanadium-nitride microalloyed steel. Mater Sci Eng A. 2014;604:117–21.
[15] Zhang C, Zhang L, Xu Q, Xia Y, Shen W. The kinetics and cellular automaton modeling of dynamic recrystallization behavior of a medium carbon Cr–Ni–Mo alloyed steel in hot working process. Mater Sci Eng. 2016;678:33–43.
[16] Chen L, Sun W, Lin J, Zhao J. Modelling of constitutive relationship, dynamic recrystallization and grain size of 40Cr steel during hot deformation process. Res Phys. 2019;12:784–92.
[17] Yan X, Chen C, Zhang XX, Dai HH, Jia JB, Bai ZH. Dynamic recrystallization kinetics and microstructure evolution of an AZ91D magnesium alloy during hot compression. Mater Charact. 2018;145:39–52.
[18] Nie X, Dong S, Wang F, Jin L, Dong J. Effects of holding time and Zener–Hollomon parameters on deformation behavior of cast Mg–8Gd–3Y alloy during double-pass hot compression. J Mater Sci Technol. 2018;34(11):69–75.
[19] Razmpoosh MH, Zarei-Hanzaki A, Imandoust A. Effect of the Zener–Hollomon parameter on the microstructure evolution of dual phase TWIP steel subjected to friction stir processing. Mater Sci Eng. 2015;638:15–9.
[20] Shang XQ, Cui ZS, Fu MW. A ductile fracture model considering stress state and Zener–Hollomon parameter for hot deformation of metallic materials. Int J Mech Sci. 2018;144:800–12.
[21] Qin FM, Zhu H, Wang ZX, Zhao XD, He WW, Chen HQ. Dislocation and twinning mechanisms for dynamic recrystallization of as-cast Mn18Cr18N steel. Mater Sci Eng A. 2017;684:634–44.
[22] Souza PM, Mendiguren J, Chao Q, Beladi H, Hodgson PD, Rolfe B. A microstructural based constitutive approach for simulating hot deformation of Ti6Al4V alloy in the α + β phase region. Mater Sci Eng A. 2019;748:30–7.
[23] Butanda JA, Málaga C, Plaza RG. On the stabilizing effect of chemotaxis on bacterial aggregation patterns. Appl Math Nonlinear Sci. 2017;2(1):157–72.
[24] Esteban M, Núñez EP, Torres F. Bifurcation analysis of hysteretic systems with saddle dynamics. Appl Math Nonlinear Sci. 2017;2(2):449–64.
[25] Gao W, Wang W. A tight neighborhood union condition on fractional (g, f, n′, m)-critical deleted graphs. Colloq Math. 2017;149:291–8.
[26] Gao W, Wang W. New isolated toughness condition for fractional (g, f, n)-critical graph. Colloq Math. 2017;147:55–65.
[27] Sudhakar S, Francis S, Balaji V. Odd mean labeling for two star graph. Appl Math Nonlinear Sci. 2017;2(1): 195–200.
[28] Zead I, Saad M, Sanad M, Bhary MM, Gadallah K, Shokry A. Photometric and spectroscopic studies of the intermediate-polar cataclysmic system DQ her. Appl Math Nonlinear Sci. 2017;2(1):181–94.